Nuclear orientation of radioactive ^{56}Mn ions implanted in the insulators $MnCl_2 \cdot 4H_2O$ and $CoCl_2 \cdot 6H_2O$

J. Pond,[1] D. Beck,[2] P. De Moor,[2] T. Phalet,[2] M. Prandolini,[2] P. Schuurmans,[2] N. Severijns,[2] T. Briant,[3] B. G. Turrell,[1] L. Vanneste,[2] B. Vereecke,[2] and S. Versyck[2]

[1]*Department of Physics and Astronomy, University of British Columbia, Vancouver, British Columbia, Canada V6T 1Z1*

[2]*Instituut voor Kern- en Strahlingsfysica, Katholieke Universiteit Leuven, 200D Celestijnenlaan, B-3001 Leuven, Belgium*

[3]*Ecole Normale Superieure, 24 rue Lhomond, F-75231 Paris, Cedex 05, France*

(Received 12 January 2000; revised manuscript received 17 April 2000)

Low-temperature nuclear orientation experiments on radioactive ^{56}Mn ions implanted into insulating, antiferromagnetic crystals of $MnCl_2 \cdot 4H_2O$ and $CoCl_2 \cdot 6H_2O$ are reported. In $MnCl_2 \cdot 4H_2O$, comparison of the γ-ray anisotropy of the ^{56}Mn nuclei with that of ^{54}Mn, doped into the sample during growth, showed that both the ^{56}Mn and ^{54}Mn spins felt a very similar hyperfine field. The site occupancy factor in a simple, two-site model was deduced to be $0.96^{+0.04}_{-0.07}$. In $CoCl_2 \cdot 6H_2O$, the average hyperfine field for the implanted ^{56}Mn was significantly less than that for ^{54}Mn and corresponded to $f = 0.53 \pm 0.10$.

I. INTRODUCTION

The great majority of experiments exploiting the technique of on-line nuclear orientation (NO) of implanted isotopes have been motivated by nuclear or fundamental physics. All experiments to date have used a metallic magnetic material, usually an Fe foil, as the host. However, from the condensed-matter point of view, there is a very wide range of magnetic materials that are insulators, and we decided to investigate the performance of these as hosts for on-line experiments. In this regard, we note that implantation of radioactive isotopes has been used to study the physics of semiconductors and insulating systems by the Mossbauer[1] and perturbed angular correlation[2] (PAC) techniques. Usually the experiments are performed off-line although there have been on-line measurements using PAC on, for example, high-temperature superconductors.[3] For nuclear orientation, on-line measurements would open the door to many new experiments to investigate interesting magnetic structures. Although NO and NMR on oriented nuclei (NMRON) have many orders of magnitude more sensitivity than conventional NMR, it is often very difficult to obtain samples doped with a suitable isotope. This problem would be obviated if an isotope could be implanted in an on-line experiment. An insulating host may also, in specific cases, provide a larger hyperfine interaction than an Fe host.

In these first experiments to investigate the efficacy of the method, we chose to implant ^{56}Mn into antiferromagnetic crystals of $MnCl_2 \cdot 4H_2O$ and $CoCl_2 \cdot 6H_2O$. $MnCl_2 \cdot 4H_2O$ is antiferromagnetic below $T = 1.6$ K. The crystal structure is monoclinic with $\beta = 99.7°$, and the magnetic easy axis (along which the magnetization is aligned in zero field) is close to the c axis. The magnetic properties have been studied by NO and NMRON using ^{54}Mn as the radioactive probe.[4–7] In fact, it was the first insulating ordered magnet in which NMRON was successfully performed.[4] $CoCl_2 \cdot 6H_2O$ is also antiferromagnetic with a similar crystallographic structure, but with $\beta = 122.3°$, and an ordering temperature of 2.3 K. The easy axis of magnetization is the c axis. In this case, the magnetism is more complicated with some orbital contribution. Previous NO studies have shown that a significant orientation of ^{56}Mn can be achieved by incorporating it as an impurity in the crystal.[8] The magnetism is close to ''spin only'' in these crystals and the hyperfine field is large with a value $B_{hf} \approx 60$ T.

Radioactive ^{56}Mn has spin $I = 3$, magnetic moment $\mu = 3.227\ \mu_N$, and a half-life $t_{1/2} = 2.6$ h. It decays by β^- emission to the daughter ^{56}Fe and the γ ray observed in the experiment is the $E2$ transition from the 2^+ 847 keV level to the $0+$ ground state. Figure 1 represents a simplified decay scheme in which only the β^- decays with intensities greater than 1% and the subsequent γ rays feeding to the observed 847 keV transition are shown.

The isotope ^{56}Mn, with $I = 3$, magnetic moment $\mu = 3.282\ \mu_N$, and a half-life $t_{1/2} = 303\ d$, was also utilized in these experiments. In this case, the decay to the daughter ^{54}Cr is by electron capture to the 835 keV level and the observed γ ray is the subsequent $E2$ transition to the $0+$ ground state. The decay scheme is shown in Fig. 2.

II. EXPERIMENTAL PROCEDURE

The crystals were grown from saturated aqueous solutions of the salts in a temperature controlled environment. The final crystals had an area of ~ 1 cm^2 and a thickness of ~ 0.2 cm. During growth, the $MnCl_2 \cdot 4H_2O$ crystal was doped with the radioactive isotope ^{56}Mn while the $CoCl_2 \cdot 6H_2O$ crystal was doped with both ^{56}Mn and ^{60}Co. These isotopes are long lived, have simple decay schemes and their γ-ray anisotropies were used both to ascertain the temperature of the crystals and to provide a comparison with the γ-ray anisotropy of the implanted isotopes.

A special sample holder was designed to clamp the crystal to the cold finger using Apiezon-N grease yet allow ~ 1 cm^2 of its face to be exposed to the ion beam. The cold finger was ''top-loaded'' into the Louvain-La-Neuve dilution refrigerator,[9] but, because the hydrated crystals deteriorate under reduced pressure at temperatures $T \geqslant 240$ K, the top-

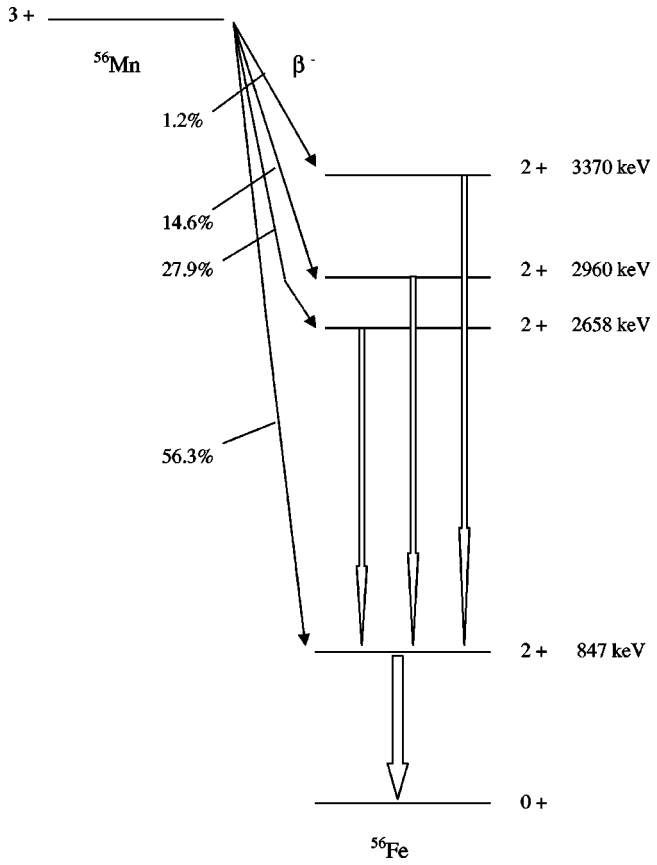

FIG. 1. Simplified decay scheme for ^{56}Mn showing the observed 847 keV γ ray and the dominant feeds to it either by direct β emission or by β emission followed by a γ ray.

loading equipment was modified to enable the crystals to be pre-cooled before insertion into the dilution refrigerator. A ^{57}Co-Fe foil was also soldered to the cold finger in order to monitor its temperature. A magnetic field, B_0 was applied not only to magnetize the ^{57}Co-Fe foil, but also to reduce the nuclear spin-lattice relaxation time, T_1, of the Mn spins and

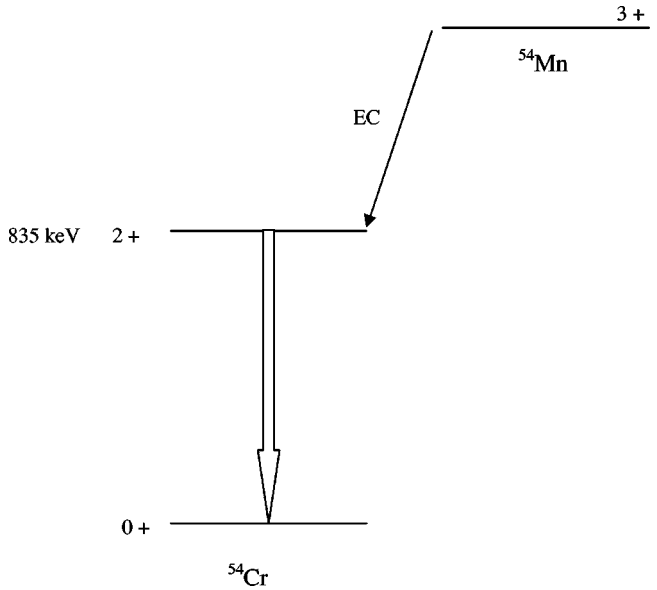

FIG. 2. Decay scheme for ^{54}Mn showing the observed 835 keV γ ray and the preceding electron capture decay.

so increase their rate of cooling.

The ^{56}Mn ions were produced at the CYCLONE cyclotron in Louvain-La-Neuve. A 100 MeV, 2.5 mA deuteron beam was directed on to a ^{55}Mn target foil mounted in an ion guide source. Reaction products recoiling out of the foil were thermalized in helium buffer gas at 200 mbar pressure inside the ion source. The positive ions leaving the source through the extraction hole were accelerated to 50 keV, mass separated and then transported to the dilution refrigerator where they were implanted at a rate $\sim 10^3$ s^{-1} into the crystal samples.

Germanium detectors were placed in various directions with respect to the crystalline axes to measure the intensities of the 835 keV γ ray in the ^{56}Mn decay (electron capture to ^{54}Cr), the predominant 847 keV γ ray in the ^{56}Mn decay, the 1173 and 1332 keV γ rays for ^{60}Co (in the ^{56}Mn-$CoCl_2 \cdot 6H_2O$ experiment) and the thermometric 122 keV transition in the ^{57}Co decay. Pulser signals were also recorded in each detector to correct for electronic dead time and to check the stability of the data acquisition system. A magnetic field, B_0, was applied in a horizontal direction, and two high efficiency detectors mounted in the horizontal plane, counted radiation emitted parallel (detector 1) and perpendicular (detector 2) to B_0. A third, lower efficiency detector monitored counts in the vertical direction, i.e., perpendicular to B_0.

In the first experiment, the $MnCl_2 \cdot 4H_2O$ crystal was oriented so that the crystalline c axis, which is close to the magnetic easy axis, was horizontal. Thus the directions of the c axis and the applied field, B_0, were parallel within the angular uncertainty of aligning the crystal that was $\pm 4°$. With this geometry, detectors 1 and 2 measured radiation emitted at angles $\theta_1 = 0°$ and $\theta_2 = 90°$, respectively. When ^{56}Mn was implanted into the sample, a problem was immediately encountered. The insulating crystals warmed up to $T \sim 100$ mK during the implantation process not due to the deposition of energy by the implanted isotopes, but because of the exposure to thermal radiation down the side access. This problem was overcome because the half-life of ^{56}Mn (2.6 h) allowed the experiment to be done pseudo-on-line in cycles. In each cycle the following operations were performed:

(i) ^{56}Mn was first implanted into the crystal for a time $> \tau_{1/2}$ so that sufficient activity built up;

(ii) The side access was closed and the system cooled for a time $> \tau_{1/2}$;

(iii) The dilution refrigerator was warmed up to a temperature $T > 100$ mK to obtain ''warm'' counts for normalization.

The cooling of the crystal is limited by the extraction of the heat capacity of the abundant nuclear spins (^{55}Mn or ^{59}Co). There are two ''bottlenecks'': the Kapitza boundary between the crystal and the copper cold finger, and the nuclear spin-lattice relaxation characterized by a time T_1. In $B_0 = 0$, the cooling is initially limited by the Kapitza resistance, but as the temperature falls, T_1 increases exponentially[7] with an exponent proportional to $(-E_g/k_B T)$ where E_g is the magnon energy gap. In order to increase the cooling rate one can utilize the ''magnon cooling'' effect.[6] B_0 is adjusted to a value very close to the ''spin-flop'' field, $B_{AE} \sim (2B_E B_A)^{1/2} \sim 0.7$ T, where B_A and

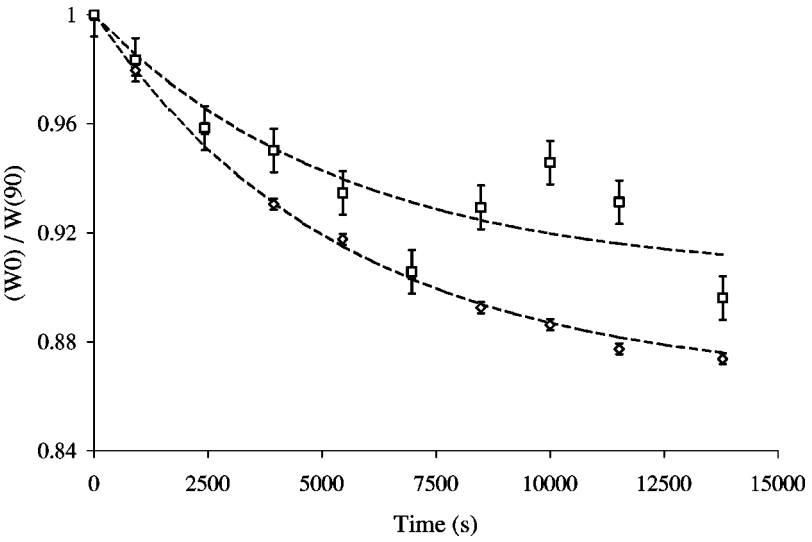

FIG. 3. Variation of the γ-ray anisotropy, $\varepsilon = W(0)/W(90)$, versus time for implanted ^{56}Mn ($\square$) and ^{54}Mn ($\diamond$) in $MnCl_2 \cdot 4H_2O$ single crystal. The dashed curve through the ^{56}Mn data is calculated from the fit through the ^{54}Mn data that is a simple exponential decay described in Eq. (4), with $f = 0.96$.

B_E are the anisotropy field and exchange field, respectively. This causes E_g to be decreased, at least for one branch of the magnons, and T_1 is much reduced.

In the second experiment ^{56}Mn was implanted into $CoCl_2 \cdot 6H_2O$ and measurements made using the same pseudo-on-line procedure discussed above. The same γ rays were counted as in the $MnCl_2 \cdot 4H_2O$ experiment as well as the 1173 and 1332 keV transitions in the ^{60}Co decay. In this case, because of the way in which the crystal grew, it was fitted into the sample holder with the *a* axis vertical. The *b* axis was horizontal and perpendicular to B_0. Thus the angular directions of detectors 1 and 2 were 32° and 90° to the easy *c*, axis, respectively, assuming exact alignment of the crystal.

III. RESULTS AND ANALYSIS

The ^{54}Mn nuclei sit at lattice sites in the crystal because the ions are incorporated into the crystals during their growth. The nuclei thus experience a unique magnetic hyperfine field, $B_{\rm hf}$, and the normalized γ-ray intensity observed at angle θ to the magnetization axis at temperature T is defined by[10]

$$W(\theta)_{54} = 1 + \sum_{k=2,4} B_k U_k A_k Q_k P_k(\cos\theta). \qquad (1)$$

The B_k are the nuclear orientation parameters which are dependent on $(\mu B_{hf}/Ik_BT)$. The U_k are deorientation coefficients which correct for transitions preceding the observed γ ray, and, for the $3+ \rightarrow 2+$ electron capture, $U_2 = 0.8281$ and $U_4 = 0.4179$. For the $E2$ 835 keV γ ray, the values for the A_k parameters are $A_2 = -0.5976$ and $A_4 = 1.0690$. The Q_k are corrections for the solid angle subtended by the detectors and are $Q_2 = 0.820$ and $Q_4 = 0.490$ for the geometry used. The P_k are the ordinary Legendre polynomials.

For implanted nuclei there is a possibility that not all of them go into lattice sites. In the case of metals (e.g., iron), this effect is usually taken into account by a simple, two-site model which assumes that a fraction f of the ions experience the full hyperfine field $B_{\rm hf}$ and a fraction $(1-f)$ feel zero field. Although the hydrated crystals used in these experiments have a more complicated crystalline structure, we assume the same model so that the normalized intensity γ-ray intensity for the ^{56}Mn nuclei is given by

$$W(\theta)_{56} = 1 + f \sum_{k=2,4} B_k' U_k' A_k' Q_k P_k(\cos\theta). \qquad (2)$$

In the ^{56}Mn decay scheme there are several preceding transitions feeding the observed 847 keV γ ray. The U_k' coefficients depend on the relative intensities of these transitions and the multipole character of the γ rays involved. The admixtures of $E2$ relative to $M1$ character into the 2523, 2113, and 1811 keV γ rays are, respectively, $\delta = 0.25 \pm 0.15$, 0.27 ± 0.03, and -0.18 ± 0.01,[11] and the resulting values for deorientation coefficients are $U_2' = 0.6391$ and $U_4' = 0.1265$. The A_k' coefficients for the 847 keV γ ray are again $A_2' = -0.5976$ and $A_4' = 1.0690$.

Note that, even if the assumptions of the two-site model are inappropriate, the factor f is still a useful parameter to describe the effect of implantation because it does describe the reduction in the γ-ray anisotropy, i.e.,

$$f = \frac{W(\theta)_{56} - 1}{W(\theta)_{56,m} - 1}, \qquad (3)$$

where $W(\theta)_{56}$ is the observed intensity and $W(\theta)_{56,m}$ is the maximum intensity that would be observed if all the ^{56}Mn ions were at substitutional sites.

In experiments on nuclei with a long half-life it is usual to measure $W(0)$ and $W(90)$, by comparing cold counts to warm counts measured in directions along the quantization axis (0°) and perpendicular to it (90°), respectively. The effect of the decay of a short lived isotope can be obviated by measuring the ratio $\varepsilon(0,90) = W(0)/W(90)$ and comparing this ratio cold and warm.

A. ^{56}Mn-$MnCl_2 \cdot 4H_2O$ experiment

Figure 3 shows the results obtained from four successful implantation/cooling/warming cycles performed in the ^{56}Mn-$MnCl_2 \cdot 4H_2O$ experiment. In each cycle counts were taken at intervals of 300 s. The values of $W(0)/W(90)$ for ^{54}Mn and ^{56}Mn obtained from the cold counts were normalized against a weighted average from warm counts taken

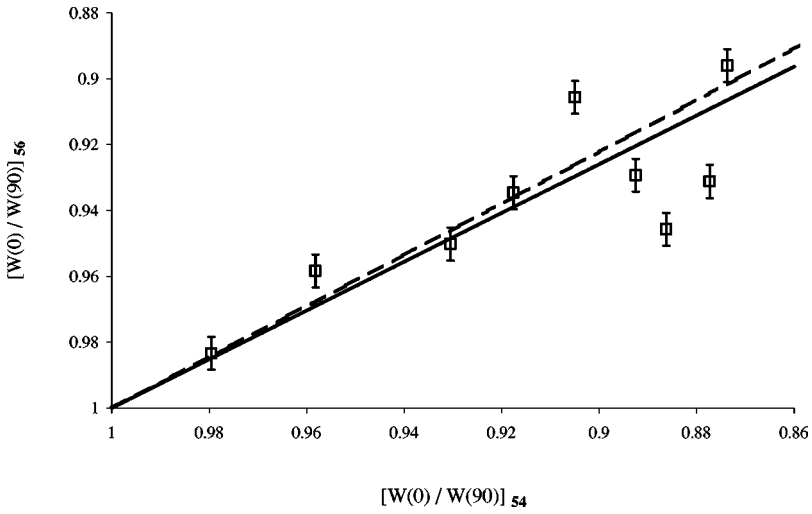

FIG. 4. The comparison of the ^{56}Mn anisotropy $W(0)/W(90)$ with that for the ^{54}Mn in a $MnCl_2 \cdot 4H_2O$ single crystal. The solid line is the best fit to the data and corresponds to a value for the lattice site occupancy $f = 0.96^{+0.04}_{-0.07}$, i.e., close to unity. The dashed line corresponds to a value for the lattice site occupancy $f = 1$.

before and after the cooling to give the anisotropy $\varepsilon(0,90)$. In each separate run counts were averaged over five consecutive 300 s intervals and then the grand average for $\varepsilon(0,90)$ taken. The lowest value of $\varepsilon(0,90)$ for ^{54}Mn, about 0.87, corresponding to a temperature $T \sim 60$ mK, was obtained in ~ 3 h. This temperature is a little higher than expected, but may have been due to extraneous heating of the crystal by thermal radiation from 4 K walls. It should be noted that even in off-line experiments with optimum heat shielding, an initial cooling of a $MnCl_2 \cdot 4H_2O$ crystal from 100 mK to a low temperature, e.g., 30 mK, takes many hours.[6]

The ^{54}Mn data can be fitted by a curve calculated from Eq. (1) with an exponential dependence on time given by

$$\varepsilon(0,90) = 1 - 0.135\left[1 - \exp\left(-\frac{t}{\tau_1}\right)\right] \tag{4}$$

with the time constant $\tau_1 = 5500$ s. This is an effective relaxation time for the cooling which, as mentioned above, is limited by the Kapitza boundary and nuclear spin-lattice relaxation. A very rough estimate using $\tau_1 = R_K C$, where the Kapitza resistance R_K, for area A, is defined[12] by $R_K A T^3 \sim 5 \times 10^{-3}$ K^4 m^2 W^{-1} and the thermal capacity C is given by $CT^2 \sim 5 \times 10^{-5}$ J K, gives a time constant of 3000 s at $T \sim 60$ mK for the crystal used, indicating that both bottlenecks are limiting the cooling. As well as the two bottlenecks, the spin-lattice relaxation involves the solution of a master equation that includes populations of the $2I$ magnetic substates and the transition rates between them.[2] Thus the simple exponential behavior described by Eq. (4) is very oversimplified because the actual relaxation process is quite complicated. However, the objective was to find a model that described the variation of the ^{54}Mn anisotropy wih time in order to determine how the ^{56}Mn anisotropy changed. The dashed curve through the ^{56}Mn data was obtained by calculating the ^{56}Mn anisotropy from the ^{54}Mn curve (see Fig. 4) using Eqs. (1) and (2) with a value $f = 0.96$, and assuming the same relaxation time, τ_1.

The comparison of $\varepsilon(0,90)$ for ^{54}Mn and ^{56}Mn is shown in Fig. 4. A least-squares analysis of the data gives the solid line corresponding to $f = 0.96^{+0.04}_{-0.07}$. The dashed line is for $f = 1$. The value obtained for f indicates that the occupancy of lattice sites by the implanted ions is very high in the two site model.

It should be noted that, even in metals, the two-site model, which is generally used for the analysis of nuclear orientation data, is rather crude. Nuclei can end up in substitutional lattice positions, in interstitial sites (and perhaps there are more than one of these), or in positions damaged by the implantation process. Thus the nuclei might feel the full hyperfine field, a reduced one, or none at all. The structure of $MnCl_2 \cdot 4H_2O$ is more complex than a metal-like iron so that there may be more nonsubstitutional sites. The $^{2+}$Mn ion has a half-filled $3d$ shell and ''spin only'' magnetism, but there are crystal-field effects that reduce the hyperfine field from that expected for the free ion value.[5] Therefore, it is likely that the hyperfine interaction for nonsubstitutional Mn ions will be different from, but possibly close to, the full value. The observed anisotropy might be due to a majority of implanted ions in substitutional sites feeling the full hyperfine field and a few experiencing zero effect (two-site model) or to many ions having a field slightly different from the full value. Future experiments using NMR experiments on the oriented nuclei (NMRON) should clarify the situation.

B. ^{56}Mn-$CoCl_2 \cdot 6H_2O$ experiment

These experiments were performed in $B_0 = 0.6$ T. Because of the alignment of the crystal, the magnetization is turned away from the easy axis towards the applied field as the latter is increased. We calculate, using the reported values for the exchange and anisotropy constants,[13] that the electronic sublattice magnetizations are turned 4° towards the direction of B_0 that is also the direction of detector 1. In this case, the angular position for the horizontal detector 1, which was at 32° to the magnetization axis in $B_0 = 04$, would be $\theta_1 = 28°$ assuming exact alignment of the crystal. The orientation of detector 2 remained $\theta_2 = 90°$. The angle θ_1 can actually be determined from the ^{54}Mn data. The plot of the normalized intensities of the ^{54}Mn γ rays measured in the two detectors is shown in Fig. 5 and the best fit to the data (dashed line) indicates that θ_1 was actually 27° instead of the

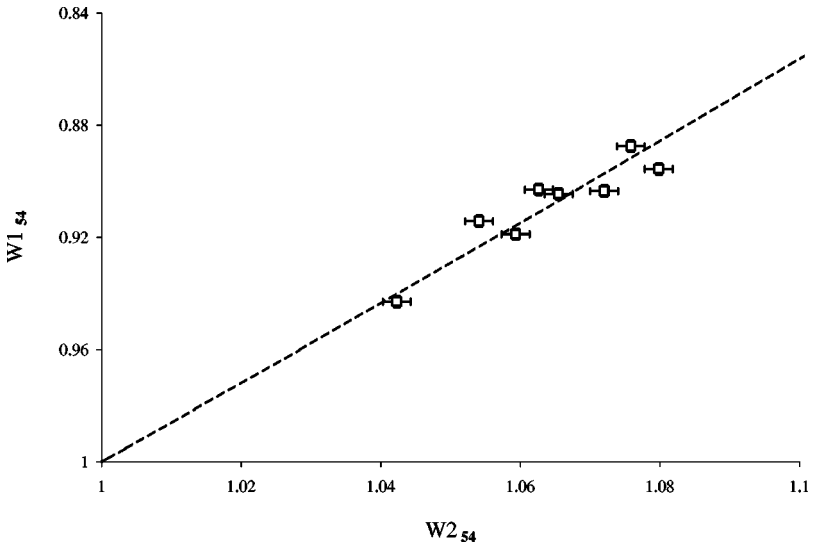

FIG. 5. The plot of the normalized intensities for ^{54}Mn measured in the two detectors. Detector 2 is at an angle of 90° to the magnetization direction and therefore measures a normalized intensity $W2=W(90)$. Because of the alignment of the $CoCl_2\cdot 6H_2O$ crystal, detector 1 is at angle θ_1 to the magnetization direction, and the best fit to the data (dashed line) shows that $\theta_1=27°$ so that $W1=W(27)$.

calculated 28°, but this difference is well within the uncertainty in aligning the crystal. For the data analysis we used the measured value $\theta_1=27°$.

The average results for four successful implantation cycles are shown in Fig. 6. The final value of $\varepsilon(27,90)=W(27)/W(90)$ corresponds to a lower crystal temperature of $T=40(2)$ mK. The dashed curve through the ^{54}Mn is a fit using a double exponential function

$$\varepsilon(27,90)=1-0.05\left[1-\exp\left(-\frac{t}{\tau_2}\right)\right]-0.15\left[1-\exp\left(-\frac{t}{\tau_3}\right)\right], \tag{5}$$

where τ_2 and τ_3 are 250 and 4000 s, respectively. This expression was chosen to fit the data, but the first term could be considered to represent the removal of ^{59}Co nuclear spin heat capacity (which is much smaller than for the ^{55}Mn heat capacity in $MnCl_2\cdot 4H_2O$ because of the much smaller hyperfine field), while the second term is due to the nuclear spin-lattice relaxation (expected to be weaker for the same reason). The dashed curve through the ^{56}Mn data is then calculated from the fit to the ^{54}Mn data using Eqs. (1) and (2) with a value for $f=0.53$ estimated from the comparison of $\varepsilon(27,90)$ for ^{54}Mn and ^{56}Mn shown in Fig. 7. The best fit for the data shown in Fig. 7 is obtained using $f=0.53\pm0.10$.

There are various explanations for the smaller ^{56}Mn γ-ray anisotropy relative to that for ^{54}Mn in the $CoCl_2\cdot 6H_2O$ experiment. Because the ^{56}Mn ions were implanted into a Co crystal host, it seems likely that fewer of them ended up in good lattice positions. The hyperfine field in interstitial sites may be less than in lattice sites. Also, the interstitial Mn spins may not have been aligned with the easy axis of the crystal. In each case, the average anisotropy of the γ rays would be reduced.

Incident thermal radiation could also cause a temperature gradient across the crystal that has quite a low thermal conductivity. The ^{56}Mn are implanted only a few hundred Å into the surface and, therefore, might be at a higher temperature than the ^{54}Mn deep in the interior. However, this reduced effect in ^{56}Mn should then also be observed in the $MnCl_2\cdot 4H_2O$ experiments. The quality of the surface might be a factor, and, indeed, the surface of the $MnCl_2\cdot 4H_2O$ was visually better than that of the $CoCl_2\cdot 6H_2O$ crystal so that in the latter there may have been a significant number of ions in damaged sites feeling a low or zero hyperfine field. Again, future experiments, measuring $W(\theta)$ vs T down to lower

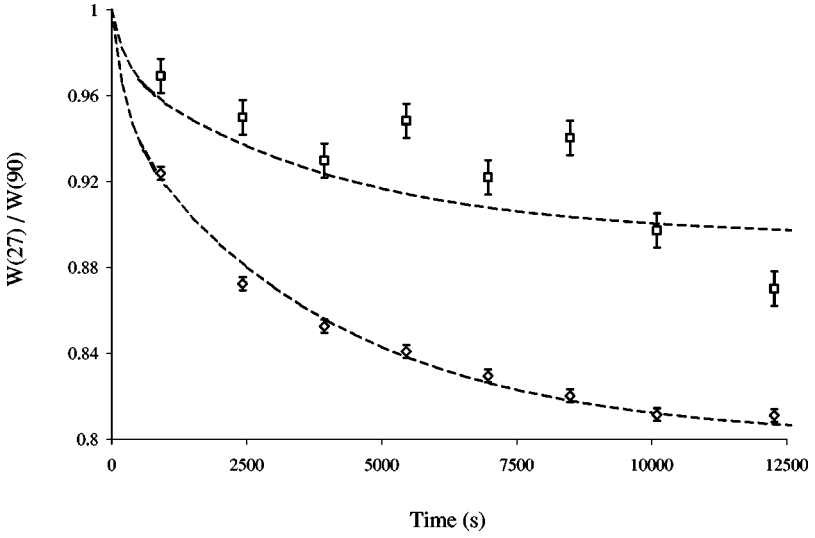

FIG. 6. Variation of γ-ray anisotropy, $\varepsilon=W(27)/W(90)$, versus time for implanted ^{56}Mn (□) and ^{54}Mn (◇) in $CoCl_2\cdot 6H_2O$ single crystal. The dashed curve through the ^{56}Mn data is calculated from the fit through the ^{54}Mn data that is the double exponential decay described by Eq. (5), with $f=0.53$.

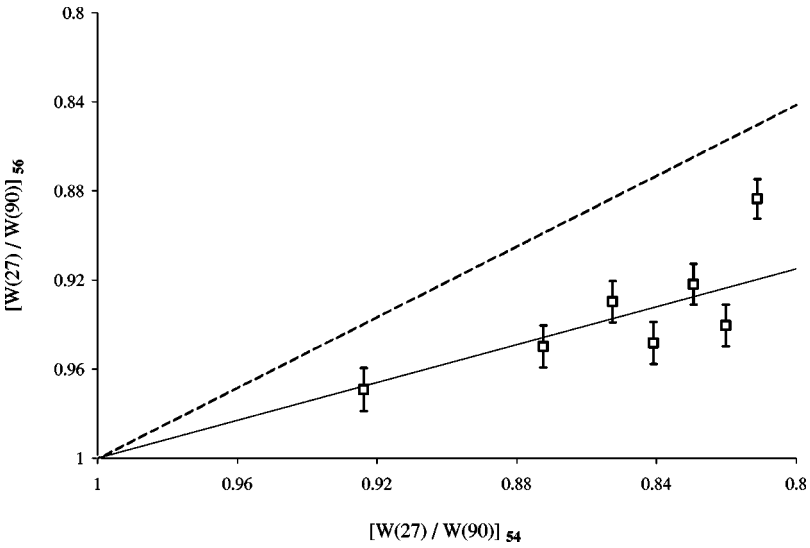

FIG. 7. The comparison of the ^{56}Mn anisotropy with that for ^{54}Mn in $CoCl_2 \cdot 6H_2O$ single crystal for the data shown in Fig. 1. Because the last two points in Fig. 6 have the same value of 0.811 for $[W(27)/W(90)]_{54}$, the average of the two $[W(27)/W(90)]_{56}$ values is taken to give the last point in this figure. The best fit is given by the solid line and gives a value of the lattice site occupancy $f = 0.53 \pm 0.10$. The dashed line corresponds to $f = 1$.

temperatures and performing NMRON would provide more precise information concerning these effects. A very small value of $\varepsilon \sim 1\%$ was measured for the ^{60}Co indicating that the hyperfine interaction in the cobalt atoms is quite small.

IV. CONCLUSIONS

Our experimental results demonstrate that radiation damage does not preclude significant γ-ray anisotropies being obtained after implantation into insulators. For ^{56}Mn implanted into $MnCl_2 \cdot 4H_2O$ an effect close to that for ^{54}Mn was observed, corresponding to $f = 0.96^{+0.04}_{-0.07}$ in the simple two-site model. This value for f might also represent a large number of ^{56}Mn ions being in sites in which the hyperfine field is less but close to the full substitutional value. It appears that the situation is similar to that in metallic hosts, in which there may be some radiation damage, but the final position of the implanted nucleus is not in the region of greatest damage. For ^{56}Mn implanted into $CoCl_2 \cdot 6H_2O$, the observed γ-ray anisotropy was significantly less than that for ^{54}Mn with $f = 0.53 \pm 0.10$. It is also shown that the long spin-lattice relaxation times that can occur in insulators does not prevent the nuclear orientation of implanted isotopes.

These experiments have demonstrated that insulators can be used as hosts for on-line experiments, at least for implanted isotopes with half-lives >1 h. Potentially, a new and exciting area for condensed-matter physics has been opened up. Interesting magnetic structures which are difficult to dope could be studied by nuclear methods by implantation of a suitable isotope.

ACKNOWLEDGMENTS

This research was supported by the Natural Sciences and Engineering Research Council of Canada (NSERC) and the Fund for Scientific Research-Flanders (FWO). We are also grateful for the support of the technical staffs at the cyclotron and isotope separator of the Catholic Universities of Louvain-La-Neuve and Leuven.

[1] See, e.g., A. Perez, G. Marest, B.D. Sawicka, J.A. Sawicki, and T. Tyliszczak, Phys. Rev. B **28**, 1227 (1983); L. Niesen, Hyperfine Interact. **13**, 65 (1983); G. Langouche, *ibid.* **84**, 279 (1994).

[2] See, e.g., J.C. Soares, Nucl. Instrum. Methods Phys. Res. B **64**, 215 (1992).

[3] Y. Kawase, S. Uehara, and S. Nasu, Hyperfine Interact. **84**, 329 (1994).

[4] A. Kotlicki and B.G. Turrell, Hyperfine Interact. **11**, 197 (1981).

[5] A. Kotlicki, B.A. McLeod, M. Shott, and B.G. Turrell, Phys. Rev. B **29**, 26 (1984).

[6] A.L. Allsop, M. de Araujo, G.L. Bowden, R.G. Clark, and N.J. Stone, J. Phys. C **17**, 915 (1984).

[7] M. Le Gros, A. Kotlicki, and B.G. Turrell, Hyperfine Interact. **77**, 203 (1993).

[8] B.G. Turrell, P.D. Johnston, and N.J. Stone, J. Phys. C **5**, L197 (1972).

[9] D. Vandeplassche, L. Vanneste, H. Pattyn, J. Geenen, C. Nuytten, and E. van Walle, Nucl. Instrum. Methods **186**, 211 (1981).

[10] See, e.g., K.S. Krane in *Low Temperature Nuclear Orientation*, edited by N.J. Stone and H. Postma (North-Holland, Amsterdam, 1986), Chap. 2.

[11] See, e.g., R. B. Firestone, *Table of Isotopes*, 8th ed., edited by V.S. Shirley (Wiley, New York, 1996).

[12] O.V. Lounasmaa, *Experimental Principles and Methods Below 1K* (Academic, New York, 1974).

[13] I.J. Lowe and D.W. Whitson, Phys. Rev. B **6**, 3262 (1972).